Cell wall composition determines handedness reversal in helicoidal cellulose architectures of *Pollia condensata* fruits

Yin Chang[a,1], Rox Middleton[a,1,2], Yu Ogawa[b], Tom Gregory[c,3], Lisa M. Steiner[a,d], Alexander Kovalev[e], Rebecca H. N. Karanja[f], Paula J. Rudall[c], Beverley J. Glover[g], Stanislav N. Gorb[e], and Silvia Vignolini[a,4]

[a]Chemistry Department, University of Cambridge, Cambridge CB2 1EW, United Kingdom; [b]Univ. Grenoble Alpes, CNRS, Cermav, Grenoble 38000, France; [c]Jodrell Laboratory, Royal Botanic Gardens, Kew, Richmond, Surrey TW9 3AB, United Kingdom; [d]Department of Plant and Environmental Sciences, University of Copenhagen 1871 Frederiksberg C, Denmark; [e]Functional Morphology and Biomechanics, Zoological Institute, Kiel University, Kiel 24118, Germany; [f]Department of Plant Sciences, Kenyatta University 43844-00100, Nairobi, Kenia; and [g]Department of Plant Sciences, University of Cambridge, Cambridge CB2 3EA, United Kingdom

Edited by Lia Addadi, Structural Biology, Weizmann Institute of Science, Rehovot, Israel; received June 25, 2021; accepted October 31, 2021

Chiral asymmetry is important in a wide variety of disciplines and occurs across length scales. While several natural chiral biomolecules exist only with single handedness, they can produce complex hierarchical structures with opposite chiralities. Understanding how the handedness is transferred from molecular to the macroscopic scales is far from trivial. An intriguing example is the transfer of the handedness of helicoidal organizations of cellulose microfibrils in plant cell walls. These cellulose helicoids produce structural colors if their dimension is comparable to the wavelength of visible light. All previously reported examples of a helicoidal structure in plants are left-handed except, remarkably, in the *Pollia condensata* fruit; both left- and right-handed helicoidal cell walls are found in neighboring cells of the same tissue. By simultaneously studying optical and mechanical responses of cells with different handednesses, we propose that the chirality of helicoids results from differences in cell wall composition. In detail, here we showed statistical substantiation of three different observations: 1) light reflected from right-handed cells is red shifted compared to light reflected from left-handed cells, 2) right-handed cells occur more rarely than left-handed ones, and 3) right-handed cells are located mainly in regions corresponding to interlocular divisions. Finally, 4) right-handed cells have an average lower elastic modulus compared to left-handed cells of the same color. Our findings, combined with mechanical simulation, suggest that the different chiralities of helicoids in the cell wall may result from different chemical composition, which strengthens previous hypotheses that hemicellulose might mediate the rotations of cellulose microfibrils.

helicoidal cell wall | chirality | structural colors | mechanical properties of plant cell wall | cellulose–hemicellulose interaction

The brightest coloration in nature is produced by reflection from nanostructures on the length-scale of visible light wavelengths. A color-generating architecture that occurs repeatedly in nature is the organization of microfibrils into helicoids (1). Such structural color is produced by cellulose helicoids in plant tissues from ferns (2, 3) to monocots (4–6) and eudicots (7) and by chitinous helicoids in the exocuticle of insects (1, 8, 9).

While the biological significance of this structural color is debated (1, 10, 11), the chirality of the helicoid has generally been considered a result of the intrinsic chirality of its constituent biomolecules. In all reports of helicoidal biomaterials, only left-handed chirality has been found, except in *Pollia condensata* (5), despite debate in wood helicoids (12). However, there is no indication of a mechanism by which left-handed structures could convey an evolutionary advantage in either mechanical or optical properties. First, under any nonrotational stress, there is no mechanical difference between structures of either handedness. Second, while structurally colored helicoids reflect circularly polarized light of the same chirality as their structure, there is very little evidence of terrestrial animal visual systems capable of detecting circularly polarized light and distinguishing the differences between reflectance of the two circular polarizations of light (13, 14). The only known exception to the left-handed chirality of reflective helicoidal architectures is reported in the epicarp of *P. condensata* fruits, in which cell walls composed of left- and right-handed helicoidal architectures are observed in different cells (5). The appearance of cell walls of opposite handednesses is surprising and begs the question why and how it should appear in this one species but not in other tissues.

Several mechanisms have been proposed for forming the oriented microfibrils in helicoidal cell walls, via biological control (15, 16), physical forces (11, 17), and the use of hemicellulose to guide the cellulose orientation (18–21). Although constraints have been found in models of cell wall growth (6), the factors

Significance

Helicoidal architectures are widespread in nature; several species adopt this structure to produce brilliant colorations. Such chiral architectures are usually left-handed in plants, with the only exception found in the cell walls of epicarp cells of *Pollia condensata*, where both handednesses are observed. Here, we aim to understand the origin of handednesses by analyzing optical and mechanical responses of single cells. Surprisingly, we discover that left-handed and right-handed cells show different distributions of spectra and elasticity. We verified by using finite element analysis simulation that the elasticity of helicoids is sensitive to the ratio of cellulose/cell wall matrix. Our findings reveal that cell wall composition affects the helicoidal architectures, suggesting that chemical composition plays a role in morphogenesis of the chirality reversal.

Author contributions: Y.C., R.M., and S.V. designed research; Y.C., R.M., Y.O., T.G., L.M.S., A.K., P.J.R., B.J.G., S.N.G., and S.V. performed research; Y.C., R.M., Y.O., and S.V. analyzed data; Y.C., R.M., Y.O., L.M.S., B.J.G., S.N.G., and S.V. wrote the paper; and R.H.N.K. contributed fruits.

The authors declare no competing interest.

This article is a PNAS Direct Submission.

[1]Y.C. and R.M. contributed equally to this work.

[2]Present address: Department of Life Sciences, University of Bristol, Bristol BS8 1TQ, United Kingdom.

[3]Present address: Institute of Archaeology, University College London, London WC1E 6BT, United Kingdom.

[4]To whom correspondence may be addressed. Email: sv319@cam.ac.uk.

This article contains supporting information online at http://www.pnas.org/lookup/suppl/doi:10.1073/pnas.2111723118/-/DCSupplemental.

Published December 15, 2021.

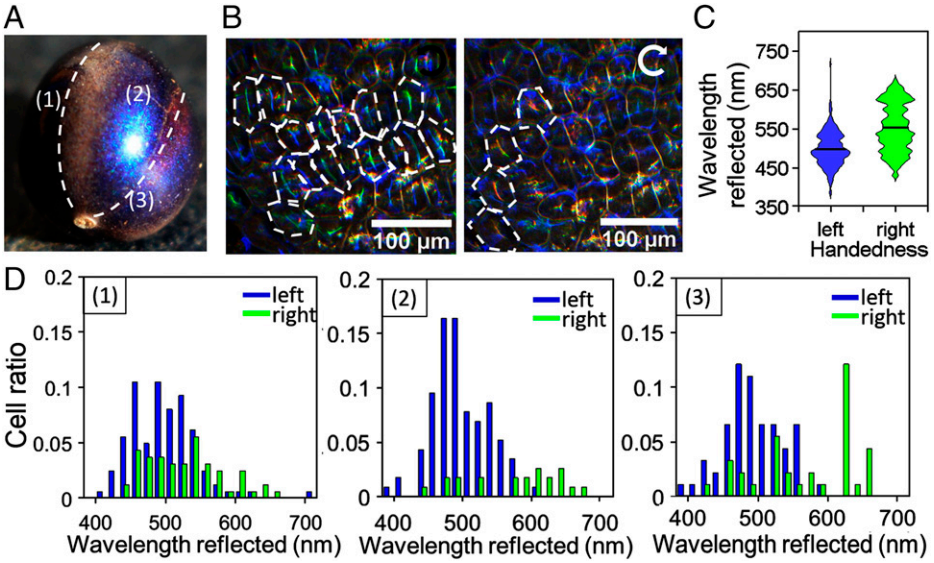

Fig. 1. Polarized coloration and distribution of differently colored left- and right-handed cells on the epicarp of *P. condensata* fruits. (*A*) *P. condensata*: slightly ovoid shaped fruit of about 4 to 5 mm in diameter exhibiting striped coloration including the following: a white interseptum stripe (1), the blue nonstripe regions (2), and a red septum stripe (3). (*B*) Polarization-resolved optical micrograph of epicarp measured using left- (black arrow) and right-handed (white arrow) polarized light, respectively. In the images, structurally colored cells are recognizable (cell contour outlined with white dashed lines). The color of the cell is seen as a line along the *Top Center* due to the curvature of the cell and the numerical aperture of the objective. (*C*) Statistical analysis of colors and chirality of cells across four fruits revealing that right-handed cells (green plot) generate more red-shifted colors than left-handed cells (blue plot). (*D*) The cell ratio of left-handed and right-handed cells with specific reflected wavelength at the three differently colored regions marked in (*A*) are calculated and normalized to the total numbers of cells. A higher proportion of right-handed cells with longer reflected wavelengths in the stripe regions (1) and (3) contribute to the white or red macroscopic coloration.

responsible for the control of handedness remain unknown. The chemical composition of the cell wall, and the interactions between cellulose and other polysaccharides within it, might play an important role in cell wall organization and chirality. Pioneering work by Reis et al. (22) has suggested the functional importance of hemicellulose in driving helicoidal architectures of cellulose in quince mucilage.

Here, to investigate the structural origin of helicoidal chirality, we compared the optical and mechanical characteristics of helicoidal *P. condensata* cell walls with different handedness. We based our analysis on the observation that the polarization of the reflected light can be used to identify the chirality of each individual cell. We observed that left-handed and right-handed cells are not evenly distributed across the fruit surface: different areas in the epicarp are dominated by different chiralities. While most of the cells reflect light in the blue spectral region, we observed that right-handed helicoidal cells have a red-shifted reflection wavelength. By performing nanoindentation on cells with known handedness, we observed that left-handed helicoids on average have higher stiffness and hardness than right-handed ones. Furthermore, independently of handedness, we observed that helicoids reflecting the longest wavelengths have greater stiffness and hardness than cells reflecting shorter wavelengths.

Results

Distribution of Cells with Different Handedness and Colors. Fig. 1*A* shows the metallic blue *P. condensata* fruit. As described by Vignolini et al. (5), the striking color of the fruit is the result of the reflection from individual cells with helicoidal cell wall architecture. When the reflected wavelength (λ), average refractive index of the material (n), and the helicoidal pitch (p) follow $\lambda = 2np$ (1, 5, 23), left-handed helicoids reflect left-handed circularly polarized light of that wavelength (11).

In *P. condensata* fruits, the epicarp appears blue with six stripes connecting the apex and calyx. Three of the stripes correspond to the internal septa, dividing the fruit into three locules. The other three stripes are spaced equidistantly and correspond to the dorsal carpellary trace or the external vascular bundle, which forms thickened tissues on the inside of the epicarp, as shown in *SI Appendix*, Fig. S1. The stripes are formed by cells with increased prevalence of longer reflective wavelength, making these regions appear more white, purple, or red than the rest of the fruit (Fig. 1*A*). These colored stripes also correspond to areas where there are higher proportions of right-handed cells. In some localized areas on the stripes, the right-handed cells make up the majority. Microscope images using a left- or a right-handed circular polarization filter show that cells with different handedness are clearly recognizable within the same small area on the epicarp (Fig. 1*B*). By taking polarization resolved spectra from more than 1,000 individual cells from four *Pollia* fruits, we confirmed that the spectral peaks reflected from right-handed cells are on average red-shifted with respect to left-handed ones as shown in Fig. 1*C* (for statistics in each fruit, see *SI Appendix*, Fig. S2).

However, as shown in the histograms in Fig. 1*D*, the distribution of left- and right-handed cells is highly variable between different regions. Cell ratios in Fig. 1*D* are calculated by dividing the amounts of specifically colored and handed cells with the total numbers of cells counted in the region. Left-handed cells (blue bars) are far more numerous in the blue regions covering most of the area of the epicarp, while right-handed cells (green bars) are mainly observed colocalized with the stripes. Similar results were obtained from four independent fruits (*SI Appendix*, Fig. S2), where 1,145 cells (369, 451, 77, and 248, respectively) were investigated.

To further demonstrate the presence of cells with different handedness in the same tissue, transmission electron microscopy (TEM) was used to image a cross-section through the epicarp, as shown in Fig. 2. In this image, several layers of thick-walled cells are visible below the external cuticle. Everywhere in the cell wall, Bouligand arcs are visible, which are characteristic of the

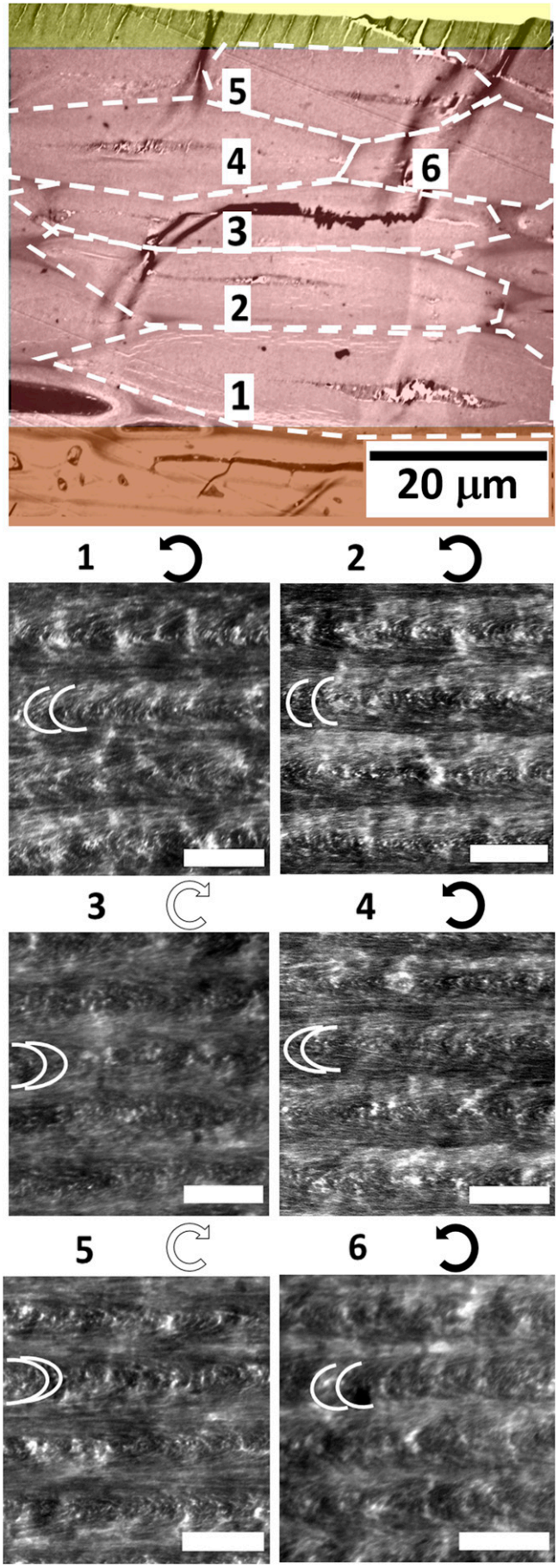

helicoidal organization of fibrous materials. The orientation (convex to the right or left) of the arcs indicates the handedness of each helicoid. On this single transect, different arc orientations may be observed in each cell, indicating that the helicoids are of opposite chirality. The electron micrographs verify the optical observations that neighboring cells are composed of cell wall architectures with opposite handedness.

Mechanical Properties and Chirality. We used nanoindentation to determine the elastic modulus (the resistance of the material to elastic deformation) and the hardness (the resistance to local deformation, a hybrid property of elastic and plastic deformations) of individual cell walls. This technique is commonly used to assess mechanical properties of biological materials with microscopic heterogeneity (24–28), as it permits measurements of local mechanical responses.

The thick waxy cuticle layer (3 to 4 μm) covering the outside of the epicarp significantly affects the nanoindentation results on cell walls (elastic modulus and hardness of untreated and cuticle-removed samples are compared in *SI Appendix*, Fig. S4 and Table S1). To indent the cell wall directly, the cuticle layer was removed by physically polishing the surface of fruits (see the cross-sectional scanning electron microscopy [SEM] image in Fig. 3*A*). Chemical etching was avoided in order to preserve the integrity of the cell wall (*SI Appendix*, Fig. S3 provides more detailed discussion of the effects of chemical treatment on the coloration and structure of fruits). As illustrated in Fig. 3*B*, the surface of the cell after cuticle removal (by polishing with Fiber Polishing Films [Thorlabs, LF03P]) with a grain size of 300 nm) was sufficiently smooth 1) to be imaged with optical microscopy and 2) to be characterized with nanoindentation with a negligible effect of surface roughness.

As illustrated in Fig. 3*B*, indentation was applied to the top surface in the center of each cell wall. The central location corresponds to the region where the reflected color was visible, indicating that the orientation of helicoids was aligned with the optical axis of the microscope objective. Continuous stiffness measurement (CSM) was used to test the mechanical responses of the cell wall continuously during nanoindentation. The elastic modulus (E) and hardness (H) of each cell are average values at deep indentation depths of 1.0 to 1.2 μm. Each indentation leaves a mark on the cell wall that is visible both on the SEM and optical images taken after indentation.

After the nanoindentation test, cells with the indents were classified by handedness and color using polarization microscopy, as shown in the four microscope photos in Fig. 3*C*. We excluded from the analysis any indentation on cell edges where the orientation of the cell wall may have been nonperpendicular to the surface, or those on cells in which the handedness was unidentifiable due to light scattering (*SI Appendix*, Fig. S5). A total of 224 of 320 indentation measurements from five different *Pollia* fruits were successfully related to the coloration and handedness of the helicoidal structure. Comparisons of the mechanical properties of the two handednesses across five fruits are shown in *SI Appendix*, Fig. S6. Statistical analyses of mechanical properties of cells with different colors and handedness are provided in *SI Appendix*, Tables S2–S5. Significantly different stiffness and hardness of cells with opposite chirality

Fig. 2. TEM images of the epicarp cross-section of a fruit of *P. condensata* and enlarged images of the cell walls of six individual cells as labeled. Different region of the epicarp, namely the cuticle layer, the region containing the structurally colored cells, and pigmented cells are shaded with different false colors of yellow, red, and brown, respectively. Note that only one handedness can be found in each cell with no mixture of handedness. Varied pitch lengths are observed in cells which explain the wide variation in reflection peak wavelength from both cell types. (Scale bar: 100 nm.)

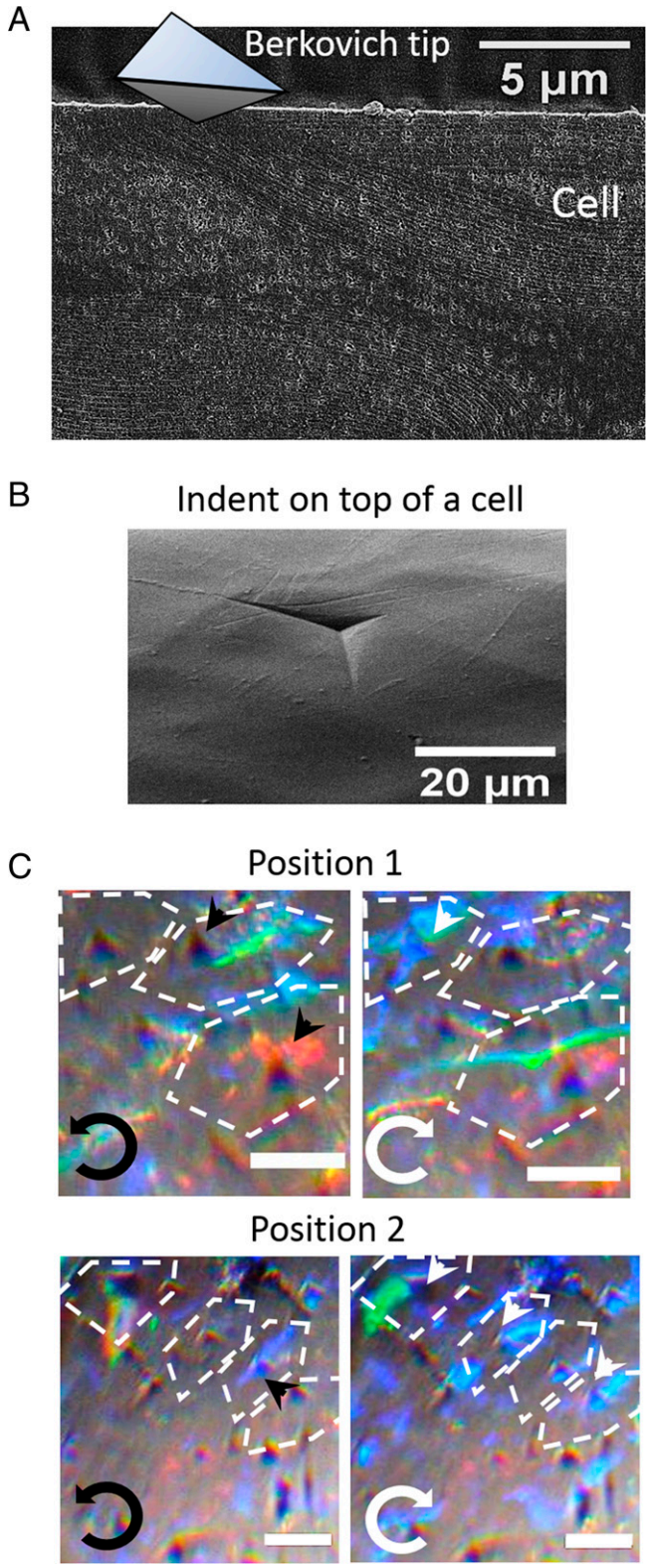

Fig. 3. Nanoindentation on cells with different colors and handedness. (*A*) SEM cross-section image of the helicoidal cell wall after removal of the outer cuticle and a schematic illustration of indentation on cells with a Berkovich tip. (*B*) The top-view SEM image shows an ideal indent at the center of a cell. (*C*) Polarization-resolved optical micrograph in two positions of epicarp measured after indentation, using left- (black arrow) and right-handed (white arrow) polarized light. Each indent indicated by arrow heads can be related to a specific color and handedness (black: left-handed; white: right-handed) of the cell. (Scale bar: 20 μm.)

was observed for blue-reflecting cells (which have a shorter pitch length).

Fig. 4*A* shows the average value of elastic modulus (E) and hardness (H) for cells with different handedness and categorized into four color ranges. The helicoidal structures with larger pitches reflect longer wavelengths and possess higher elastic modulus (E), which means the cell walls are stiffer. A difference of the moduli of cells ($\Delta E_{\text{max-min}}$) with larger and smaller pitches is observed regardless of handedness ($\Delta E_{\text{max-min, left-handed}} = 1.15$ GPa, $\Delta E_{\text{max-min, right-handed}} = 1.94$ GPa). Surprisingly, for cells reflecting short wavelengths, the left-handed cells show a significantly higher E than right-handed cells. This means that for cells with similarly small pitch lengths, those with cellulose microfibrils (CMFs) rotated left-handedly are stiffer than right-handedly rotated ones. Similarly, H is higher for left-handed helicoids than right-handed ones at short wavelengths. The average value of H remains the same for both handednesses (within error) for cells with long reflection wavelengths (cells with larger pitch). The larger error for the value of E and H in longer pitch (red-shifted) left-handed cells is due to lower sample numbers as red cells are predominantly right-handed (*SI Appendix*, Table S2); however, they do not contradict the trends observed in the shorter wavelength categories.

Interestingly, from the plot in Fig. 4*B* reporting H as a function of E, we observe that among biomaterials with a stiffness of 1 to 20 GPa, the hardness of the cell wall of *P. condensata* fruits (for all colors and handednesses) is comparable with the highest values observed in some biomaterials adapted for both hardness and stiffness, such as teeth, beaks and mandibles (29, 30). The correlation of the hardness and stiffness are discussed in *SI Appendix*. We further investigated the factors that contribute to these outstanding mechanical properties of the cells using computational modeling.

Using finite element analysis (FEA) we computed a spherical indentation of composites composed of helicoidally arranged CMFs in a cell wall matrix to understand how the following factors contribute to the stiffness of helicoids: 1) the filling fraction of CMFs (the remainder being cell wall matrix), 2) the diameter of the CMF, and 3) the twisting angles of the CMF layers. The architectures of computational models are based on the helicoidal organization of secondary plant cell walls suggested by Reis et al. (22). The strategy for FEA model construction is described in *SI Appendix*, and the FEA model is schematized in *SI Appendix*, Fig. S8. In these models, a larger twisting angle between the CMF layers results in a smaller pitch when the fibril diameter and the filling fraction are constant. Readers are referred to *SI Appendix*, *Finite element models and simulation method for indentation test* for detailed simulation methods and parameters.

Fig. 4*C* shows the computed stiffness obtained from the models with CMF diameters of 3 or 4 nm and with pitches ranging from 120 to 220 nm by varying fiber orientations of 3 to 14° (details are described in *SI Appendix*). The darker points in Fig. 4*C* denote the stiffness of helicoids with larger pitch lengths. There is no correlation between pitch length and stiffness (values of stiffness of helicoids with different fiber orientations are shown in *SI Appendix*, Fig. S9). In contrast, the average stiffness of the cell wall varies strongly with CMF diameter and the filling fraction of CMFs in the composite. These results indicate a strong correlation between the stiffness of the cell walls and their composition but no correlation between the stiffness and the orientation of CMFs in the helicoid.

Discussion

We have shown that cells with different handedness have not only different spatial locations on the fruit epicarp but

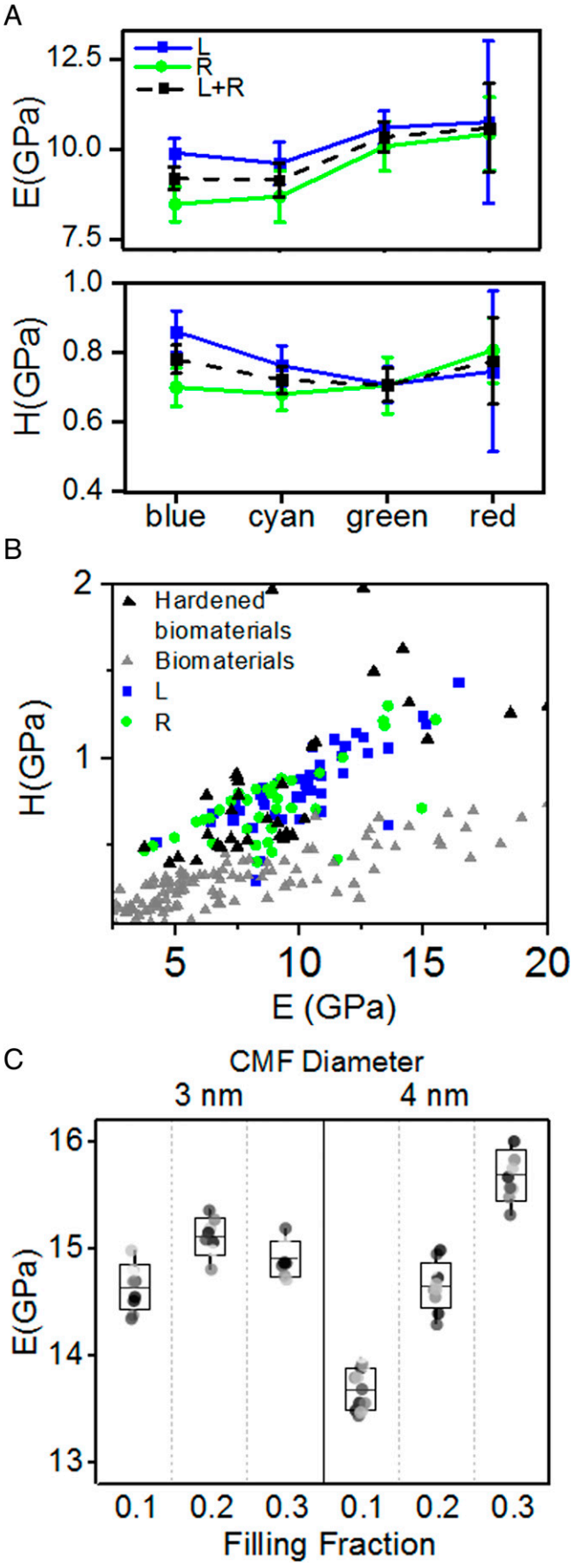

significantly different distributions of reflected colors and mechanical properties. The key question with regard to the presence of right-handed cells in this species is how they came to differentiate from left-handed cells in the same tissue and from all other known examples of cellulose helicoids.

We observed differences in the mechanical properties of the cells in their elastic modulus (elastic deformation) rather than in their hardness (plastic deformation). To understand the elastic deformation, we therefore use a model in which the cell wall was approximated as a composite of CMFs within a mechanically homogenous single-component matrix. This approximation is justified because, as in many other secondary cell walls (31), the cell wall of *P. condensata* is primarily composed of three main components: cellulose, hemicellulose, and lignin, as confirmed by solid-state NMR spectroscopy and Fourier-transform infrared spectroscopy of the epicarp (*SI Appendix*, Fig. S12). We consider the matrix to consist of a combination of hemicellulose and lignin (see also *SI Appendix* discussion for details on the motivation for this choice). However, we speculate that hemicelluloses are playing a more important role than lignin in the organization of CMFs and therefore the development of handedness. This is because lignification occurs only after deposition of cellulose and hemicelluloses (32, 33), and lignin is considered to have very limited interactions with CMFs. In other words, the formation of the helicoidal architecture occurs when CMFs are deposited into largely hemicellulosic cell wall matrix.

The FEA analysis suggests that the average stiffness of cell wall composites depends on the diameter of the CMFs and the proportion of the matrix rather than on the twisting angle between CMFs. The diameter of CMFs, while varying between plants, is well defined within a specific tissue (34–36). This is also the case for the helicoidal cell wall of *P. condensata* based on cross-sectional TEM observation of CMFs (*SI Appendix*, Fig. S11 and Table S5). We therefore associate the different mechanical properties with a different amount or composition of the matrix. Moreover, the FEA shows that for equal cell wall compositions, left-handed and right-handed helicoids should demonstrate the same mechanical properties. In contrast, in Fig. 4 we observe higher mechanical strength in left-handed cell walls than in right-handed cells for a given pitch, indicating a difference in composition between the two cell types.

Although we do not have direct evidence that composition is a causal factor (as this would require a quantitative analysis of the polysaccharides in individual cell walls), the evidence here supports the idea that composition affects helicoid architecture

Fig. 4. Measured and simulated mechanical properties of the cellulose cell walls (blue marks for left-handed and green marks for right-handed cells). (*A*) Experimentally measured reduced modulus, *E*, as a function of the handedness and color of the helicoids. On average (the black dashed line), red-shifted cells have higher reduced modulus*, *E*. The reduced modulus takes into account the elastic deformation in both the surface of the sample and the tip of the indenter during contact. Here, the deformation of the tip is ignored, so the reduced modulus relates to the Young's modulus (E_y) and Poisson's ratio (v) of the sample: $E = E_y/(1 - v^2)$. A similar trend is shown for both chiralities despite the fact that left-handed cells are stiffer than the same color right-handed cells. Hardness, *H*, of differently colored cells is constant at 0.7 to 0.8 GPa. (*B*) The mechanical properties of general biological materials (light gray triangles) and of some specifically hardened biological materials (black triangles). Data are collected from literature across eight taxonomies (30). *Pollia* fruits have cell walls with high stiffness comparable to hardened biomaterials. (*C*) Computationally calculated stiffness of models with CMF diameter of 3 or 4 nm with varied filling fraction of 0.1, 0.2, or 0.3, respectively, and pitch lengths from 120 to 220 nm (represented by spots with different greyness: the darker spots indicate models with larger pitch lengths). The maximum and minimum values of stiffness in each condition were labeled on the graph.

and therefore its development. We contend that our data extend this idea to the possibility that cell wall composition has the capacity to redefine helicoid chirality.

The molecular chirality of cellulose is well defined, and so is that of CMF. On the other hand, variation in hemicellulose ratios and decorations are a potential source of opposite chirality in charge or physical symmetry. We speculate that such a difference in hemicellulose could lead to a different interaction with CMF and therefore drive the handedness inversion seen here.

Our hypothesis might also be supported by the fact that right-handed cells are predominantly observed corresponding to the vascularized and connective tissues of the whole fruit. The occurrence of distinct groups of right-handed cells in these regions could indicate that their development is linked to that of the carpellary trace tissue. Given the functional properties of these tissues in controlling transport through the fruit, this could provide an advantage to an adaptation in cell wall matrix composition. This might be an indication of the conditions under which the cells differentiate.

Alternative to this hypothesis, changes in cell wall composition might be the result of a separate causative effect which also produces chirality reversal during morphogenesis. This additional effect of any alternative theory of chirality control would be of significant interest in understanding the morphogenesis, nevertheless, producing differences in cell wall components in parallel with the extraordinary right-handed helicoidal structure.

From a biological perspective, the fact that cells with both types of handedness are observed in a single tissue remains very intriguing. In fact, there is no evident functional advantage conveyed by the handedness reversal in some cells. Unfortunately, there is insufficient knowledge about the fruit's visual ecology to know whether there is a relevant fruit-dispersing animal capable of distinguishing polarization, although it seems unlikely given the apparent rarity of this ability in nature. There may, however, be a visual signaling advantage to redder cells or the stripe pattern. Additionally, the changes in stiffness and hardness within the epicarp or with particular reference to vascular tissues could possibly convey an advantage. There may be further features of the changes in cell wall composition for enhanced functionality, such as changes in hydrophobicity or transport (37). To move beyond speculation, significant further evidence would be required.

In conclusion, we have fully analyzed the optical and mechanical differences between left- and right-handed helicoidal cellulose cell walls at the single cell level. We have correlated mechanical properties with internal structure and found higher average elastic modulus in left-handed cells compared with the same color of right-handed cells. This suggests different cell wall matrix compositions in the cell walls. This observation supports the previous hypothesis by Reis (22), who speculated that hemicellulose plays a role in the organization of cellulose helicoids in the cell wall. We believe a reasonable extension of this concept is that cell wall composition affects the handedness of the helicoid as well. There remain, of course, other mechanisms that might produce a change in both chirality and cell wall composition, while not being a causative link between composition and handedness. We present the cell wall composition theory as a plausible, well-grounded, and parsimonious explanation of the phenomenon. This is an experimental demonstration of correlation between the composition and helicoidal architecture of cell walls and their handedness. Further studies may reveal additional supporting or conflicting evidence.

Given the extreme rarity of right-handed helicoids in natural fibrillar materials, this discovery provides evidence that the handedness of the cell wall might be regulated by cell wall composition, providing additional insight to the long-debated problem of the development of helicoidal plant cell walls. The direct determination of left- or right-handedness by cell wall composition is not proven by this evidence, as the change in cell wall composition might be a secondary effect of a separate and unidentified determining factor. However, this compelling evidence of an interaction between cell wall composition and architecture indicates potential future work in confirming or refuting this causative relationship.

Materials and Methods

(a) Optical Microscopy and Image Analysis. Optical microscopy was performed using a Zeiss Axio Scope optical microscope in Köhler illumination. The microscope was equipped with a 20× objective lens (Zeiss EC Epiplan Apochromat, numerical aperture (NA) = 0.6) coupled to a spectrometer (Avantes HS2048) via an optical fiber (Thorlabs, FC-UV100-2-SR) (detection spot with diameter of ~10 μm). Spectra were normalized with a silver mirror (Thorlabs, PF10-03-P01). An additional numerical aperture in the incident beam constrained the incident light to ±5° angular variation from the optical axis. The combined effect of the cell curvature, the constrained incident angle, and the numerical aperture of the objective lens is the appearance of a narrow line-shaped reflection spot along the center of each epicarp cell. For measurements taken in left or right circular polarized light, a quarter waveplate (Thorlabs 25 mm) was mounted below an output linear polarizer and controlled independently by a motorized rotation stage (Thorlabs PRM1Z8) via Advanced Positioning Technology (APT) software.

For the cell color and handedness survey, each fruit was mounted with Blu-Tack on a glass slide to expose the measurement area at the top and placed under the microscope. Locations on the fruit surface were chosen in order to survey the front, middle, and back of a septum stripe, a dorsal carpellary trace stripe, and an area between the stripes. At each position, the microscope was focused on an area of cells in cross-polarization in order to not bias the proportion of left and right reflectance. A boundary was defined around the observation area, and every cell within that boundary measured by focusing the spectrometer on its central reflectance spot in right- or left-handed circular polarized configuration.

(b) Nanoindentation. Mature *P. condensata* fruits were collected under permit [Kenya Forest Service Material Transfer: ref. No. RESEA/1/KFS VOL.11(115)] from mature plants in Kakamega forest, Kenya. The epicarp of collected fruits was fractured to small fragments ($<1 \times 1$ mm^2). The fragments were then carefully stuck on a sample holder with superglue (5925 Elastomer, Ergo). After that, the thick cuticle (~3.5 μm) was firstly scraped off from the outermost layer of the *P. condensata* epicarp by corundum polishing paper (Buehler) with 9-μm grain size followed by polishing samples using polishing paper with 0.3-μm grain size. The removal of the cuticle was carried out and inspected via stereomicroscopy (Leica M205 A). The surface roughness was examined via fast-scanning 3D measurement microscopy (Keyence VR 3100). This preparation procedure enabled us to directly indent on cell walls and reduce surface roughness effects on nanoindentation results.

The nanoindenter (SA2, MTS Nano Instrument) equipped with a diamond Berkovich tip operated in displacement control mode, and samples were loaded under constant velocity of 30 nm/s. The CSM mode was used with an oscillation frequency of 75 Hz and amplitude of 1 nm. The maximum indentation depth was set at 2 μm, and the maximum indentation force was 23 mN. The materials' Poisson's ratio was assumed to be 0.3. Effective Young's modulus (E_R) and hardness were automatically calculated in the built-in software of the nanoindenter using the Oliver–Pharr method (38). We averaged the values of effective Young's modulus for the indentation depth of the last 200 nm (i.e., 0.8 to 1.0 μm for 1-μm maximal indentation depth and 1.8 to 2.0 μm for 2-μm maximal indentation depth).

(c) EM Sample Preparation and Imaging. The untreated fruit epicarps were broken into small pieces. Untreated fragments or polished fragments of epicarps were embedded in catalyzed London resin (LR) white acrylic resin (Agar Scientific Ltd.) and hardened overnight at 60 °C. After resin embedding, the embedded sample block was transversely cut with a 45° diamond knife (Diatom) equipped on an ultramicrotome Leica EM UC6 (Leica Microsystems). The sample block was transferred onto a SEM stub and coated with 10 nm Pt for imaging. The SEM (Tescan MIRA3 FEG-SEM) used to observe the top view was operated at 3 kV with a working distance of 5.2 mm and using an in-beam secondary electron detector.

Ultrathin sections with a thickness of 100 nm were produced and transferred onto carbon coated Cu grids (Agar Scientific Ltd). The TEM (Hitachi H-7650 TEM) equipped with an AMT 2k × 2k digital camera system was operated at 80 kV. For the width measurement, ultrathin sections of thickness of

30 to 50 nm were prepared and transferred onto carbon-coated Cu grids. The observation was done in a low-dose condition using a JEM 2100Plus TEM (Jeol Ltd.) operated at 200 kV and equipped with a Gatan Rio16 camera (Gatan, Inc.). For *SI Appendix*, Fig. S1, untreated epicarp fragments were mounted on carbon tape with cross-sections exposed and sputter-coated with 10 nm Au/Pd.

(d) Indentation Simulation. Finite element models with helicoidal layers of CMFs embedded in a cell wall matrix were constructed, and the Hertzian models in analyzing spherical indentation data were used to calculate the shear moduli. Two possible diameters of CMFs, of 3 nm or 4 nm, three filling fractions of CMFs of 0.1, 0.2, and 0.3, and, in each case, CMF layer twisting at small angles from 3° to 10° with the corresponding pitch lengths of 120 to 220 nm were computed. The spherical indenter model with a radius of 32 nm was used to allow the linear elastic analyses at the indentation depth of 1 to 1.5 μm under the constraint of the Hertzian model. Stress and displacement at the indentation depths were extracted for computing the moduli, and thick models (~60 nm) were constructed to avoid possible substrate effects. The longitudinal modulus of 150 GPa and transverse modulus of 35 GPa of each CMF and 10 GPa of cell wall matrix were used as the intrinsic material properties which are derived from molecular dynamic simulation (readers are referred to *SI Appendix* for detailed discussion).

Data Availability. Data have been deposited in "Research data supporting "Cell wall compositions determine handedness reversal in helicoidal cellulose architectures of *Pollia condensata* fruits"" (available at the University of Cambridge data repository http://doi.org/10.17863/CAM.71834).

ACKNOWLEDGMENTS. This work was supported by the Engineering and Physical Sciences Research Council (EPSRC) NanoDTC EP/G037221/1 and EP/R513179/1 (R.M.), Cambridge Trust, Biotechnology and Biological Sciences Research Council (BBSRC) David Phillips Fellowship BB/K014617/1, European Research Council (ERC) SeSaME ERC-2014-STG H2020 639088 (S.V.), and the Cambridge-Africa ALBORADA Research Fund (R.M., R.H.N.K., and S.V.). We would also like to thank Wilberforce Okeka for his help in locating fruit in the Kakamega forest. The NanoBio-Institut de Chimie Moléculaire de Grenoble (NanoBio-ICMG) platform (FR 2607) is acknowledged for granting access to the electron microscopy facility.

1. B. D. Wilts, H. M. Whitney, B. J. Glover, U. Steiner, S. Vignolini, Natural helicoidal structures: Morphology, self-assembly and optical properties. *Mater. Today Proc.* **1**, 177–185 (2014).
2. K. S. Gould, D. W. Lee, Physical and ultrastructural basis of blue leaf iridescence in four Malaysian understory plants. *Am. J. Bot.* **83**, 45–50 (1996).
3. R. M. Graham, D. W. Lee, K. Norstog, Physical and ultrastructural basis of blue leaf iridescence in two neotropical ferns. *Am. J. Bot.* **80**, 198–203 (1993).
4. G. Strout *et al.*, Silica nanoparticles aid in structural leaf coloration in the Malaysian tropical rainforest understorey herb Mapania caudata. *Ann. Bot.* **112**, 1141–1148 (2013).
5. S. Vignolini *et al.*, Pointillist structural color in Pollia fruit. *Proc. Natl. Acad. Sci. U.S.A.* **109**, 15712–15715 (2012).
6. R. Middleton *et al.*, Using structural colour to track length scale of cell-wall layers in developing Pollia japonica fruits. *New Phytol.* **230**, 2327–2336 (2021).
7. L. M. Steiner *et al.*, Structural colours in the frond of *Microsorum thailandicum*. *Interface Focus* **9**, 20180055 (2019).
8. L. Fernández Del Río, H. Arwin, K. Järrendahl, Polarizing properties and structure of the cuticle of scarab beetles from the Chrysina genus. *Phys. Rev. E* **94**, 012409 (2016).
9. C. Åkerlind *et al.*, Scattering and polarization properties of the scarab beetle Cyphochilus insulanus cuticle. *Appl. Opt.* **54**, 6037–6045 (2015).
10. K. R. Thomas, M. Kolle, H. M. Whitney, B. J. Glover, U. Steiner, Function of blue iridescence in tropical understorey plants. *J. R. Soc. Interface* **7**, 1699–1707 (2010).
11. A. Neville, S. Levy, "The helicoidal concept in plant cell wall ultrastructure and morphogenesis" in *Biochemistry of Plant Cell Walls*, C. T. Brett, J. R. Hillman, Eds. (CUP, 1985), pp. 99–124.
12. B. A. Meylan, B. G. Butterfield, Helical orientation of the microfibrils in tracheids, fibres and vessels. *Wood Sci. Technol.* **12**, 219–222 (1978).
13. M. Blahó *et al.*, No evidence for behavioral responses to circularly polarized light in four scarab beetle species with circularly polarizing exocuticle. *Physiol. Behav.* **105**, 1067–1075 (2012).
14. P. Brady, M. Cummings, Differential response to circularly polarized light by the jewel scarab beetle Chrysina gloriosa. *Am. Nat.* **175**, 614–620 (2010).
15. R. Gutierrez, J. J. Lindeboom, A. R. Paredez, A. M. C. Emons, D. W. Ehrhardt, Arabidopsis cortical microtubules position cellulose synthase delivery to the plasma membrane and interact with cellulose synthase trafficking compartments. *Nat. Cell Biol.* **11**, 797–806 (2009).
16. A. R. Paredez, C. R. Somerville, D. W. Ehrhardt, Visualization of cellulose synthase demonstrates functional association with microtubules. *Science (80-.)* **312**, 1491–1495 (2006).
17. J. Chan, Microtubule and cellulose microfibril orientation during plant cell and organ growth. *J. Microsc.* **247**, 23–32 (2012).
18. Y. Kurata *et al.*, Variation in hemicellulose structure and assembly in the cell wall associated with the transition from earlywood to latewood in Cryptomeria japonica. *J. Wood Chem. Technol.* **38**, 254–263 (2018).
19. H. Yi, V. M. Puri, Architecture-based multiscale computational modeling of plant cell wall mechanics to examine the hydrogen-bonding hypothesis of the cell wall network structure model. *Plant Physiol.* **160**, 1281–1292 (2012).
20. U. Kutschera, The growing outer epidermal wall: Design and physiological role of a composite structure. *Ann. Bot.* **101**, 615–621 (2008).
21. A. C. Neville, A pipe-cleaner molecular model for morphogenesis of helicoidal plant cell walls based on hemicellulose complexity. *J. Theor. Biol.* **131**, 243–254 (1988).
22. D. Reis, B. Vian, Helicoidal pattern in secondary cell walls and possible role of xylans in their construction. *C. R. Biol.* **327**, 785–790 (2004).
23. E. J. Warrant, Polarisation vision: Beetles see circularly polarised light. *Curr. Biol.* **20**, R610–R612 (2010).
24. S. O. Andersen, Insect cuticular sclerotization: A review. *Insect Biochem. Mol. Biol.* **40**, 166–178 (2010).
25. J. F. Vincent, U. G. Wegst, Design and mechanical properties of insect cuticle. *Arthropod Struct. Dev.* **33**, 187–199 (2004).
26. S. Büsse, S. N. Gorb, Material composition of the mouthpart cuticle in a damselfly larva (Insecta: Odonata) and its biomechanical significance. *R. Soc. Open Sci.* **5**, 172117 (2018).
27. S. O. Andersen, Chlorinated tyrosine derivatives in insect cuticle. *Insect Biochem. Mol. Biol.* **34**, 1079–1087 (2004).
28. S. O. Andersen, "Cuticular sclerotization and tanning" in *Insect Molecular Biology and Biochemistry*, L. I. Gilbert, Ed. (Academic Press, 2012), chap. 6, pp. 167–192.
29. B. W. Cribb *et al.*, Hardness in arthropod exoskeletons in the absence of transition metals. *Acta Biomater.* **6**, 3152–3156 (2010).
30. D. Labonte, A.-K. Lenz, M. L. Oyen, On the relationship between indentation hardness and modulus, and the damage resistance of biological materials. *Acta Biomater.* **57**, 373–383 (2017).
31. D. J. Cosgrove, M. C. Jarvis, Comparative structure and biomechanics of plant primary and secondary cell walls. *Front Plant Sci* **3**, 204 (2012).
32. M. J. Meents, Y. Watanabe, A. L. Samuels, The cell biology of secondary cell wall biosynthesis. *Ann. Bot.* **121**, 1107–1125 (2018).
33. N. D. Bonawitz, C. Chapple, The genetics of lignin biosynthesis: Connecting genotype to phenotype. *Annu. Rev. Genet.* **44**, 337–363 (2010).
34. M. C. Jarvis, Structure of native cellulose microfibrils, the starting point for nanocellulose manufacture. *Philos. Trans.- Royal Soc., Math. Phys. Eng. Sci.* **376**, 20170045 (2018).
35. S. Elazzouzi-Hafraoui *et al.*, The shape and size distribution of crystalline nanoparticles prepared by acid hydrolysis of native cellulose. *Biomacromolecules* **9**, 57–65 (2008).
36. H. Niimura, T. Yokoyama, S. Kimura, Y. Matsumoto, S. Kuga, AFM observation of ultrathin microfibrils in fruit tissues. *Cellulose* **17**, 13–18 (2010).
37. O. M. Terrett, P. Dupree, Covalent interactions between lignin and hemicelluloses in plant secondary cell walls. *Curr. Opin. Biotechnol.* **56**, 97–104 (2019).
38. G. M. Pharr, W. C. Oliver, Measurement of thin film mechanical properties using nanoindentation. *MRS Bull.* **17**, 28–33 (1992).